Anttu, Nicklas

Absorption of light in a single vertical nanowire and a nanowire array

Published in:
Nanotechnology

DOI:
10.1088/1361-6528/aafa5c

Published: 18/01/2019

Document Version
Peer-reviewed accepted author manuscript, also known as Final accepted manuscript or Post-print

Please cite the original version:
Anttu, N. (2019). Absorption of light in a single vertical nanowire and a nanowire array. *Nanotechnology*, *30*(10), Article 104004. https://doi.org/10.1088/1361-6528/aafa5c

Absorption of light in a single vertical nanowire and a nanowire array

Nicklas Anttu

Department of Electronics and Nanoengineering, Aalto University, PO Box 13500, FI-00076, Aalto, Finland

E-mail: nicklas.anttu@aalto.fi

Abstract

Both a single III-V semiconductor nanowire and an array of such nanowires have shown promise for solar cell applications. However, the correspondence between the optical properties of the single nanowire and the nanowire array has not been studied. Here, we perform electromagnetic modeling of InP nanowires to study this relationship. We find that a single nanowire can show at an absorption peak a remarkably high absorption cross-section that is more than 50 times the geometrical cross-section. With optimization of the diameter of the single nanowire, the short-circuit current density is 30 times higher than in a bulk solar cell. With such a strong absorption, we predict an apparent efficiency >500 % for the single nanowire solar cell. In contrast, we show that an efficient nanowire array solar cell cannot rely on strong absorption just through the absorption peak. Instead, the nanowires need to be packed rather closely to enhance the absorption of the full solar spectrum. At the optimum diameter for the nanowire array, neighboring nanowires compete strongly for absorption of incident photons at the absorption peak, which limits the absorption per nanowire by a factor of 18. As a result, the single InP nanowire is optimized at a diameter of 110 nm while the nanowires in the array are optimized at a considerably larger diameter of 180 nm. Importantly, we show analytically the coupling efficiency of incident light into the fundamental HE_{11} guided mode and consecutive absorption of the mode in the nanowires. With that analysis, we explain that a single nanowire shows two different absorption pathways — one through coupling into the guided mode and another by coupling into the nanowire through the sidewall. This analytical analysis also shows at which period the neighboring nanowires in an array start to compete for absorption of incident photons.

1. Introduction

Direct bandgap III-V semiconductor nanowires have shown promise as building blocks for absorption-based optoelectronic applications like solar cells [1-5] and photodetectors [6]. Typical size of such nanowires is comparable to the wavelength of light. Then, the optical response is dominated by diffraction of light [7-11], and absorption measurements showed that an array of nanowires absorb also the light that would travel between the nanowires in a ray-optics regime [12]. Similarly, a single nanowire can absorb light that would travel adjacent to it in a ray-optics regime [5,13].

To highlight the impact of the nanowire geometry in such a diffraction-dominated regime, we showed through optics modeling how the absorption per volume III-V material can vary by a factor of 200 in a nanowire array, mainly depending on the nanowire diameter [8]. The nanowires showed 20 times stronger absorption than bulk material. This enhanced absorption was due to efficient in-coupling into the fundamental, guided HE_{11} mode in the nanowires and consecutive strong absorption of the mode in the nanowires [7,8,14]. The HE_{11} mode is the guided mode that shows up at the longest wavelength for a given nanowire diameter [15] and hence is the mode in a single-mode nanowire fiber.

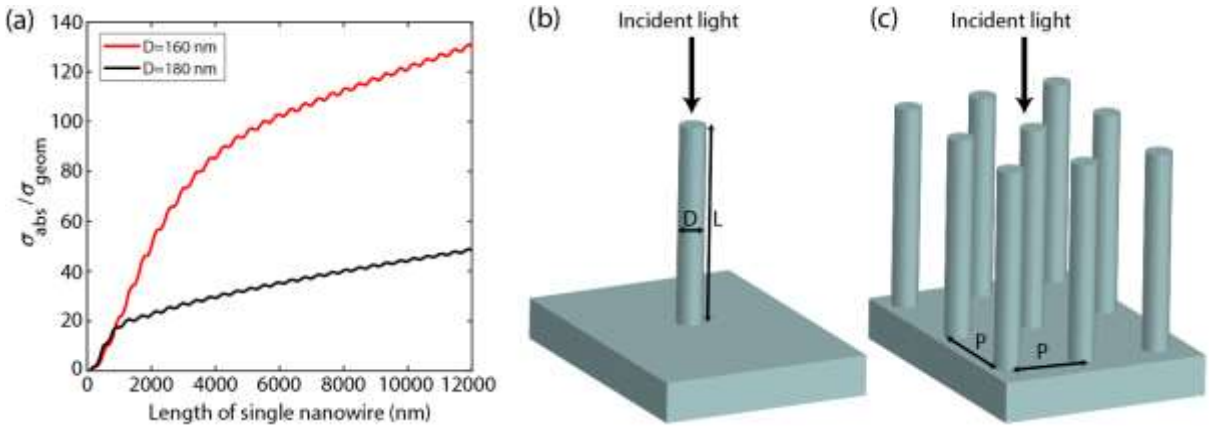

Figure 1. (a) Absorption cross-section σ_{abs}, normalized to the geometrical cross-section $\sigma_{geom} = \pi(D/2)^2$, of the single InP nanowire in (b) at a wavelength of λ = 850 nm. Note that the periodic, minor oscillations are due to interference of the incident light with the light reflected from the substrate surface, with period of $\Delta L = \lambda/2$ = 425 nm as expected for light propagating in the air on top of the substrate. (b) Schematic of a single nanowire of diameter *D* and length *L* and (c) corresponding square array of nanowires of period *P*.

For large-area applications, arrays of vertical nanowires are commonly used (Figure 1(c)) [1-4]. In such an array, each individual constituent nanowire is an active element. Therefore, also a single nanowire can be studied as a miniaturized optoelectronic device (Figure 1(b)). Thanks to an optical antenna effect, a single, vertical GaAs nanowire solar cell showed in measurements a short-circuit current density of 180 mA/cm^2 [5], which is 6 times higher than that of the record-efficiency bulk GaAs solar cell [16]. Due to this high short-circuit current density, the single nanowire solar cell showed an

apparent efficiency of 40 % [5], which is beyond the 33 % Shockley-Queisser efficiency limit of a conventional single-junction bulk solar cell [17]. Furthermore, through optics modeling, a very high short-circuit current density of >800 mA/cm^2 has been predicted for a single vertical nanowire [18].

However, the correspondence between the optical properties of an individual, vertical direct-bandgap III-V semiconductor nanowire and the corresponding nanowire array has not been studied. Here, we perform electromagnetic modeling of the absorption in a single nanowire and the corresponding array. By increasing the period of the array, we show how the behavior of the nanowires in the array converge to that of the single nanowire.

For the single nanowire, we find two absorption mechanisms. For short nanowire lengths, absorption is dominated by guided optical modes, excited at the top of the nanowire. However, after the guided modes have been absorbed, the absorption continues by coupling into the nanowire through the sidewall. We find examples where the HE_{11} mode dominates absorption up to a nanowire length of 1000 nm, beyond which the sidewall absorption starts to show up more and more, and at a nanowire length of 4000 nm, the sidewall absorption contributes half of the total absorption. Importantly, we estimate analytically the in-coupling into the HE_{11} mode and the absorption of this mode, which allows an enhanced understanding of the optical response.

We find that the absorption in a nanowire array resembles that of the single nanowire when the period is comparable or larger than the nanowire length. In an array with a small period, neighboring nanowires compete for absorption, limiting the number of absorbed photons per nanowire. For intermediate values of the array period, neighboring nanowires can scatter light in such a way that the in-coupling into the nanowires is enhanced. Then, the absorption is stronger compared to that in the individual nanowire. From the analysis of the in-coupling into the HE_{11} mode in the individual nanowires, we explain why the array shows an optimum period for absorption at a given wavelength. At that period, the coupling into the HE_{11} mode is optimized, which maximizes the absorption and minimizes the reflection.

When considering the absorption of sunlight, our modeling shows a remarkably high short-circuit current density $j_{sc,NW}$ in a single, individual nanowire. For a 2000 nm long InP nanowire of 110 nm in diameter, we find $j_{sc,NW}$ in excess of 930 mA/cm^2, which is 30 times higher than the bulk limit of 31 mA/cm^2. We predict for such a nanowire an apparent solar cell efficiency of 500 %.

However, when placing these nanowires in an array, neighboring nanowires start to compete in absorption when the array period decreases below 1000 nm. Also from the analytically calculated in-coupling into the HE_{11} mode, we predict this period of 1000 nm for the onset of the competition in

absorption. In an array with 1000 nm in period, such nanowires of 110 nm in diameter cover 1% of the surface. Then, with the $j_{sc,NW}$ = 930 mA/cm^2 short-circuit current density in the cross-section of the nanowires, we predict a short circuit-current density of $j_{sc,array}$ = 9.3 mA/cm^2 for the array, in excellent agreement with fully numerical modeling of the nanowire array.

To increase $j_{sc,array}$, the period needs to be decreased. Then, the neighboring nanowires start to compete for absorption of incident light at the wavelength that gave the absorption peak for the single nanowire. Hence, $j_{sc,array}$ increases with decreasing period, but $j_{sc,NW}$ drops and shows the value of 53 mA/cm^2 at the period of 140 nm where $j_{sc,array}$ shows the maximum value of 26 mA/cm^2. Importantly, the diameter of 110 nm that optimizes $j_{sc,NW}$ does not optimize $j_{sc,array}$. Instead, as previously shown [7], the optimum diameter for the nanowires in the array is considerably larger at 180 nm.

2. Modeling methods

The light scattering is analyzed with the Maxwell equations with light an electromagnetic wave. The optical properties of the InP nanowires and the InP substrate are taken into account through tabulated values of the wavelength-dependent complex-valued refractive index n_{InP} [19]. A non-zero value for Im(n_{InP}) indicates absorption, and the bulk absorption length is given by $1/(4\pi \mathrm{Im}[n_{InP}(\lambda)]/\lambda)$ where λ is the wavelength of light in vacuum. The incident light is a plane-wave, incident at normal angle, that is, parallel to the nanowire axis, with electric field $|\mathbf{E}_{inc}|$=1 V/m.

For the single nanowire, we use the finite-element method in Comsol Multiphysics and perform a background-field/scattered-field type of modeling. For the background field, we use the analytical solution for the Maxwell equations. This analytical solution we obtain from the Fresnel equations for the system without the nanowire. Then, in the next step, we include the nanowire and solve for the scattered field based on the background field. To model a single nanowire, we place perfectly matched layers (PMLs) in all three directions at the edges of the simulation domain. The absorption in the nanowire is calculated from the power dissipation, which is, for positions **r** within the nanowire, given by $(2\pi c/\lambda)\varepsilon_0 \mathrm{Im}(n_{InP}(\lambda))\mathrm{Re}(n_{InP}(\lambda))|\mathbf{E}(\mathbf{r}, \lambda)|^2$ where ε_0 is the permittivity of vacuum and c the speed of light in vacuum [8]. For the nanowire array, we use the scattering matrix method [20] for calculating the spectral response similarly as in Refs. [7,8]. For calculation of the electric field distribution in the nanowire array, we use the finite-element method in Comsol Multiphysics.

3. Results

First, in Section 3.1, we consider the absorption at a fixed wavelength in a single nanowire. There, we focus on the dependence of the absorption on the diameter and length of the nanowire. In Section 3.2, we consider how the period of a nanowire array affects the absorption and compare to the

behavior of the single nanowire. In Section 3.3, we turn to study the absorption of broadband sunlight. We consider especially the short-circuit current density $j_{sc,NW}$ in the cross-section of a single nanowire. We compare $j_{sc,NW}$ to $j_{sc,array}$, which is the short-circuit current density in a large-area nanowire array solar cell. In Section 3.4, we discuss the impact of the nanowire material on the absorption in the single nanowire, using GaAs and Si nanowires as examples in addition to the InP nanowires.

3.1. Absorption in a single nanowire

We start by considering a single InP nanowire of D = 180 nm in diameter. Nanowires of such a diameter, when placed in an array, optimize the absorption in large-area solar cells [7]. This optimized absorption is due to the HE_{11} mode in the nanowires, which for D = 180 nm enhances the absorption in the vicinity of the bandgap where the absorption is usually weak. Therefore, also for the single nanowire, we focus first on λ = 850 nm, which is just below the bandgap wavelength of 925 nm of InP at room temperature (corresponding to bandgap energy of 1.34 eV).

For a single nanowire and normally incident light, two distinct cross-sections exist: the geometrical cross-section of the top surface, $\sigma_{geom} = \pi D^2/4$, and the absorption cross-section, σ_{abs}. The absorption cross-section shows from how large area the nanowire appears to absorb light. That is, the power absorbed at wavelength λ by the nanowire is given by $dP_{abs}(\lambda) = \sigma_{abs}(\lambda) I_{inc}(\lambda) d\lambda$. Here, $I_{inc}(\lambda)$ is the spectral irradiance of the incident light (with units W/m^2nm).

In Figure 1(a), we show the absorption in the nanowires, in terms of $\sigma_{abs}/\sigma_{geom}$. This $\sigma_{abs}/\sigma_{geom}$ shows from how large area, relative to the geometrical cross-section, the nanowire appears to absorb light. For short nanowires, we notice a rapid increase in absorption with increasing nanowire length L. This rapid absorption settles, after which, a slower increase in absorption shows up with further increase of the length. This behavior indicates two different absorption mechanisms. For D = 180 nm, the initial, strong absorption settles at approximately 1000 nm in length where $\sigma_{abs}/\sigma_{geom} \approx 20$. For comparison, when we decrease the diameter to 160 nm, we find a much stronger absorption overall, and a settling of the strong initial absorption at a length of approximately 3000 nm where $\sigma_{abs}/\sigma_{geom} \approx 70$.

To understand these two absorption regimes and the strong diameter dependence in absorption, we have analytically estimated the in-coupling of light into the HE_{11} guided mode at the top end-facet of the nanowire (Supplementary Information Figure S1). Note that the guided modes must be excited at the end facets of the nanowire since these modes have a larger k-vector than the light in the surrounding medium [15]: Diffraction at an end facets can give rise to the required momentum increase.

We have calculated also the absorption length of the HE_{11} mode analytically (Supplementary Information Figure S1). For D = 180 nm, we find a maximum in-coupling corresponding to 18 times σ_{geom} and an absorption length of 280 nm (Supplementary Information Figure S1). For D = 160 nm, we find a higher maximum in-coupling corresponding to 61 times σ_{geom} and a longer absorption length of 860 nm (Supplementary Information Figure S1). These analytically estimated in-coupling strengths and absorption lengths of the HE_{11} mode match well with the $\sigma_{abs}/\sigma_{geom} \approx 20$ and 70 and the approximately 1000 nm and 3000 nm long regions of the initial strong absorption (about 3 absorption lengths is needed to absorb 95% of the energy in the mode) for D = 180 nm and 160 nm, respectively, in Figure 1(a). Due to this good agreement with the analytical estimates, we assign this initial strong absorption to absorption through the HE_{11} mode.

Importantly, the absorption with increasing nanowire length beyond this initial, strong absorption cannot be analyzed based on guided modes: For D = 160 nm and D = 180 nm at λ = 850 nm, only the HE_{11} mode is guided in the InP nanowire [15]. Hence, we assign the continued increase in σ_{abs} with increasing nanowire length, at lengths beyond which the HE_{11} mode has been absorbed in Figure 1(a), to light that is funneled into the nanowire through the sidewalls of the nanowire. See Supplementary Information Figure S2 for further increasing nanowire length, up to 80 µm, where the linear increase in absorption continues. Such a linear behavior is in contrast to the sub-linear behavior from the Lambert-Beer law for absorption in bulk-like samples, which is of the form $1-\exp(-\alpha L)$ with α the absorption coefficient.

To support this claim of absorption through both the HE_{11} mode and through sidewall in-coupling, we show the electric field distribution $|\mathbf{E}|^2$ for a 4000 nm long nanowire of 180 nm in diameter in Figure 2(a) — as described in Section 2, the absorption in the nanowire is proportional to $|\mathbf{E}|^2$. Here, we see how the HE_{11} mode is absorbed in the top-most 1000 nm of the nanowire, after which a more constant absorption sets in. Note that the absorption is modulated by the reflection from the substrate interface, which is seen also as the periodic, minor oscillations in the length-dependent absorption spectrum in Figure 1(a) – see Supplementary Information Figure S2 for an example without the substrate present. Thus, thanks to the sidewall in-coupling, there is no upper limit on how much a single nanowire can absorb as the nanowire length increases. As an example, from Figure 1(a) we see that for a nanowire of 4000 nm in length and 180 nm in diameter, half of the absorption at λ = 850 nm originates from the guided HE_{11} mode and half from the sidewall in-coupling.

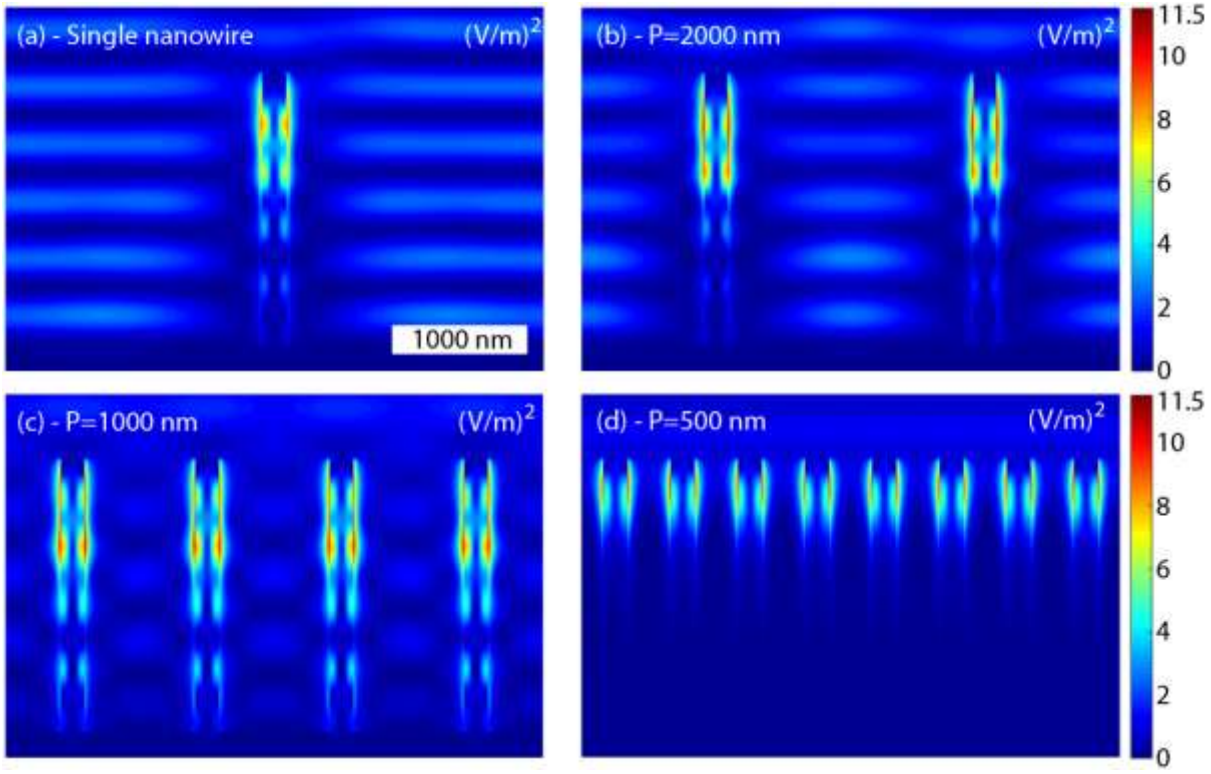

Figure 2. Electric field distribution $|\mathbf{E}|^2$ for nanowires with L = 2000 nm and D = 180 nm at λ = 850 nm for (a) a single nanowire and a nanowire array with (b) P = 2000 nm, (c) P = 1000 nm, and (d) P = 500 nm. Here, the top-most 200 nm of the substrate is shown at the bottom. This side-view is through the middle of the nanowires. Light is incident from the top side at normal angle with $|\mathbf{E}_{inc}|^2 = 1$ (V/m)^2 and polarized parallel to this side-view plane. The scale bar in (a) is 1000 nm and applies also for (b)-(d).

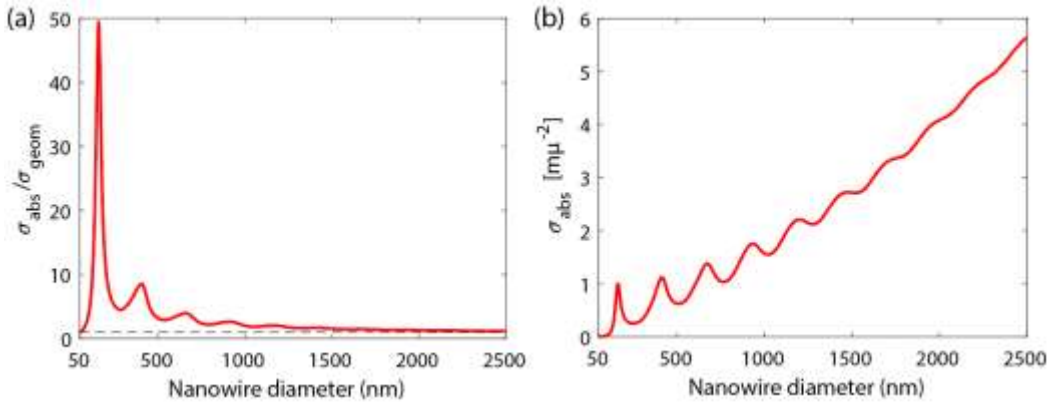

Figure 3. Absorption in a single InP nanowire of L = 2000 nm at λ = 850 nm. (a) Absorption cross-section normalized to geometrical cross-section. (b) Absorption cross-section.

To investigate the effect of different guided modes on the nanowire absorption, we show in Figure 3 the absorption as a function of nanowire diameter for L = 2000 nm and λ = 850 nm. The HE_{11} peak at D = 160 nm shows the largest $\sigma_{abs}/\sigma_{geom}$ value of almost 50 — the length dependence at this peak was

investigated in Figure 1(a). The peaks due to higher order guided modes at larger D show more moderate values. With increasing diameter, the absorption appears to settle toward values close to one. Note that from geometrical optics, we expect a settling toward values of approximately 0.7, limited by the geometrical cross-section σ_{geom} of the top surface and additionally by the ≈30% reflection from the $n \approx 3.5$ InP at that top surface [8].

When considering the number of absorbed photons, which is proportional to σ_{abs} (Figure 3(b)), nanowires with a diameter above 600 nm absorb more than the D = 160 nm nanowire at the HE_{11} peak. That is, for large-diameter nanowires, the absorbed power increases with σ_{geom}, as expected from geometrical optics. Thus, the highest ratio of the number of absorbed photons to the amount of semiconductor material used, that is, $\sigma_{abs}/\sigma_{geom}$, is reached at the HE_{11} peak, but a larger number of incident photons can be absorbed if sufficiently large diameter can be allowed for.

3.2 Absorption in a nanowire array

For a nanowire array, the absorption cross-section for each nanowire is given by $\sigma_{abs}(\lambda)/\sigma_{geom} = A(\lambda)P^2/(\pi D^2/4)$. Here, $A(\lambda)$ is the absorptance of the array, that is, the fraction of incident light that is absorbed by the nanowires. Hence, $\sigma_{abs}/\sigma_{geom}$ is maximally $P^2/(\pi D^2/4)$ for the nanowires in the array.

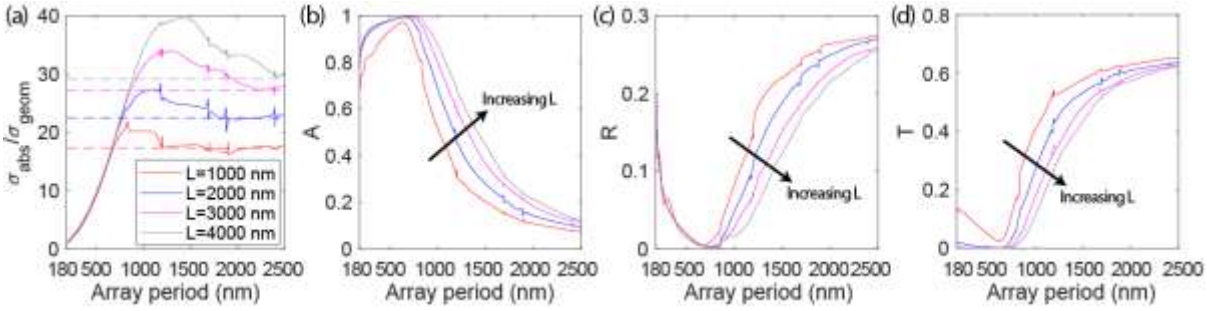

Figure 4. (a) Absorption cross-section normalized to geometrical cross-section of InP nanowires of D = 180 nm in diameter and length L in an array of period P. The dashed lines show corresponding value for a single nanowire. Here, also the absorptance (b), reflectance (c), and transmittance (d) of the array is shown with the same color-coding for L as in (a).

In Figures 4(a) and 4(b), we show for D = 180 nm the $\sigma_{abs}/\sigma_{geom}$ and A for varying nanowire length and array period (similar behavior was found also for D = 160 nm, the second diameter considered in Figure 1(a); not shown). For completeness, we show also the reflectance R of the array and the transmittance T into the substrate (Figures 4(c) and 4(d)). First, we find sharp peaks and/or dips at the positions of the Rayleigh anomalies where a diffracted order in the air top-side changes from propagating to evanescent [21]. For normally incident light, this transition occurs when $P = (m^2+n^2)^{1/2}\lambda$ where m and n are integers. For the λ = 850 nm in Figure 4, these anomalies are predicted at P = 850, 1202, 1700,

1901, and 2404 nm, in good agreement with the location of the peaks and/or dips in the spectra. Note that here, Rayleigh anomalies do not show up for the diffracted orders in the substrate – the absorption in the substrate dampens the possibility for such resonances.

With increasing period in Figure 4, the nanowires affect the overall light scattering of the array-system less and less: *A* decreases, *R* converges toward the ≈30% reflectance of the planar InP substrate of approximately 3.5 in refractive index, and *T* toward the 70% transmittance into the substrate.

For a period below 500 nm, the absorption cross-section of each nanowire in the array, σ_{abs}, in Figure 4(a) is almost independent of the nanowire length since the absorptance *A* is close to 1 (Figure 4(b)), and consequently *R* and *T* are close to zero (Figures 4(c) and 4(d)). Also, σ_{abs} for the nanowires in the array is here considerably lower than for the corresponding single nanowire (marked by the dashed lines in Figure 4(a)). That is, for these small-period arrays, neighboring nanowires compete for the absorption of incident photons and limit the absorption in each nanowire. See Figure 2(d) for $|\mathbf{E}|^2$ when *P* = 500 nm and *L* = 2000 nm. In this case, the field distribution in the nanowires is rather different from that in the single nanowire in Figure 2(a) – in the array, light does not reach the bottom of the nanowires, limiting $|\mathbf{E}|^2$ and hence the absorption per nanowire, that is, σ_{abs}. Note that a similar competition for a pair of close-lying nanowires of dissimilar diameter was observed in Ref. [22].

When $P \approx L$, we find a good agreement between σ_{abs} for the nanowires in the array and for the single, individual nanowire (Figure 4(a)). By comparing the electric field distribution in the single nanowire and the array of *P* = 2000 nm when *L* = 2000 nm (Figures 2(a) and 2(b)), we see how the nanowires in the array behave almost like individual, single nanowires.

In-between these results of strong competition in absorption at small period and single-nanowire like absorption at large period, the array can absorb stronger, per nanowire, than the single nanowire. See Figure 4(a) where, at these intermediate *P*, σ_{abs} for the nanowires in the array is above the σ_{abs} of the corresponding single nanowire. For example, for *L* = 2000 nm, at $P \approx 1000$ nm, the array absorbs ≈20% more photons per nanowire than the single nanowire. Thus, here, the nanowires scatter light in such a way that more light couples into each nanowire. See Figure 2(c) where $|\mathbf{E}|^2$ in the nanowires of the array with *P* = 1000 nm is higher, especially in the bottom half of the nanowires, than in the single nanowire in Figure 2(a).

Finally, the peak in *A* at $P \approx 700$ nm in Figure 4(b), which shows up for all modeled nanowire lengths, can be understood in terms of the analytically estimated in-coupling into the HE_{11} mode. For the *D* = 180 nm, the unit cell area P^2 is equivalent to $\approx 20\sigma_{geom}$. As discussed in Section 3.1, the individual nanowires showed an in-coupling into the HE_{11} mode that was equivalent to $18\sigma_{geom}$. Thus, $P \approx 700$

nm maximizes the coupling into the HE_{11} mode. Furthermore, the HE_{11} mode showed an absorption length of 280 nm. Thus, in these nanowires of $L \geq 1000$ nm, we expect that practically all the light that is coupled into the HE_{11} mode is absorbed.

Hence, the $P \approx 700$ nm optimizes the in-coupling into the well-absorbed HE_{11} mode in the array. For smaller P, the reflection starts to increase (Figure 4(c)), limiting A. For larger P, the in-coupling cross-section to the HE_{11} mode is below the unit cell area. Then, with increasing P, an increasing fraction of the incident light cannot be coupled to the well-absorbed HE_{11} mode, as apparent from the increasing T (Figure 4(d)) and decreasing A.

3.3 Broadband absorption for photovoltaics

Above, to study the underlying response of the nanowires, we considered the single-wavelength behavior. Such single-wavelength absorption is relevant for example for a narrow-band photodetector that is detecting a specific, possibly communication, wavelength. In contrast, for photovoltaic applications, we are focused on absorption of sunlight, which is broadband.

For a single nanowire, the number of absorbed photons is given by

$$n_{\mathrm{ph}} = \int_{\lambda_{\mathrm{low}}}^{\lambda_{\mathrm{high}}} \frac{\sigma_{\mathrm{abs}}(\lambda)\, I_{\mathrm{inc}}(\lambda)}{hc/\lambda}\, d\lambda \qquad (1)$$

where h is Planck's constant. For λ_{high} we assume the bandgap wavelength of InP of 925 nm at room-temperature, which corresponds to the bandgap energy of 1.34 eV. For I_{inc}, we use the AM1.5D 900W/m^2 direct and circumsolar spectrum [23], for which $\lambda_{\mathrm{low}} = 280$ nm, below which there is negligible intensity. If we assume that each absorbed photon contributes one charge carrier to the short-circuit current I_{sc} in the nanowire, then $I_{sc} = qn_{ph}$ with q the elementary charge. That is, we assume perfect collection efficiency of photogenerated carriers inside the solar cell. For the single nanowire, the short-circuit current density in the cross-section of the nanowire is given by $j_{sc,NW} = I_{sc}/\sigma_{geom} = I_{sc}/\pi(D/2)^2$.

For a nanowire array, the absorptance $A(\lambda)$ determines the short-circuit current density:

$$j_{\mathrm{sc,array}} = q \int_{\lambda_{\mathrm{low}}}^{\lambda_{\mathrm{high}}} \frac{A(\lambda)\, I_{\mathrm{inc}}(\lambda)}{hc/\lambda}\, d\lambda. \qquad (2)$$

Importantly, $j_{\mathrm{sc,array}}$ is the externally observed current density of the nanowire array when considered as a large-area solar cell. Then, for the square nanowire array considered here, with one nanowire per unit cell of area P^2, the current-density through the cross-section of each nanowire is given by $j_{\mathrm{sc,NW}} = j_{\mathrm{sc,array}} P^2/\pi(D/2)^2$.

For an InP nanowire array, we have shown that $D \approx 180$-200 nm optimizes $j_{sc,array}$, irrespective of the nanowire length — see Figure 6(a) in Ref. [7]. With such a diameter, the HE_{11} absorption peak enhances absorption just below the bandgap wavelength where the absorption coefficient of the semiconductor material is the weakest. The absorption at shorter wavelengths is optimized by tuning the period. The optimum period increases with nanowire length (see Figure 6(a) in Ref. [7]). When moving to the single nanowire, the period disappears as an optimization parameter.

Nanowires with $L \approx 2000$ nm are considered in solar cell applications [1,2,4,24], and we show example results for a single nanowire with $L = 2000$ nm in Figure 5.

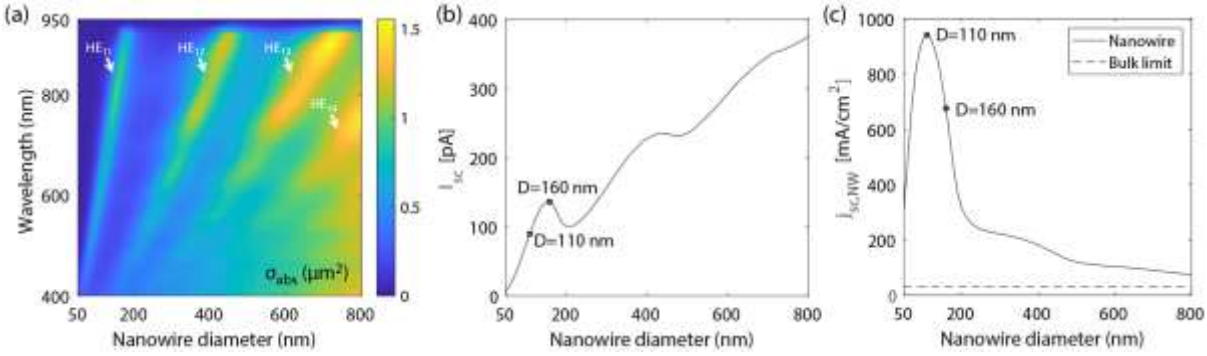

Figure 5. (a) Absorption cross-section σ_{abs} of a single InP nanowire of $L = 2000$ nm. (b) The resulting $I_{sc} = qn_{ph}$ for the single nanowire, as calculated from σ_{abs} in Eq. (1). (c) The short-circuit current density $j_{sc,NW} = I_{sc}/\pi(D/2)^2$ in the cross-section of the nanowire. The dashed line shows the 31 mA/cm^2 limit of bulk InP, which is obtained by using $A = 1$ in Eq. (2).

First, regarding the absorption cross-section (Figure 5(a)), we find peaks due to the HE_{11}, HE_{12}, and HE_{13} mode, similarly as in Ref. [22] where $D < 400$ nm was considered. Here, with increasing D, we find also a peak due to the HE_{14} mode as indicated in Figure 5(a). Out of the guided modes, normally incident light can excite only the HE_{nm} and EH_{nm} modes with odd n [7]. Excitation of the HE_{nm} and EH_{nm} modes with even n, as well as the TE_{0m} and TM_{0m} modes, is symmetry forbidden [7]. Furthermore, the overlap of the incident light with the HE_{1m} modes is larger than with the other symmetry allowed modes [7]. Hence, we see the clearest absorption peaks due to the HE_{1m} modes.

For this single nanowire, the short-circuit current I_{sc} shows a peak at $D = 160$ nm due to the HE_{11} absorption peak (Figure 5(b)) (furthermore, we see a weaker peak in I_{sc} due to the HE_{12} absorption peak at $D = 430$ nm and a much weaker peak due to the HE_{13} absorption peak at $D = 710$ nm). Thus the HE_{11} peak in I_{sc} of the single nanowire shows up in close vicinity of the $D = 180$ that optimizes $j_{sc,array}$ in the nanowire array [7]. However, in contrast to the behavior of $j_{sc,array}$ in the nanowire array, I_{sc} for the single nanowire is larger for $D > 300$ nm than at this HE_{11} peak, and I_{sc} continues to increase with increasing D [similarly as σ_{abs} at the single wavelength in Figure 3(b)].

When we turn to study the $j_{sc,NW}$ as a function of D (Figure 5(c)), we find a peak at D = 110 nm, that is, for a D considerably smaller than the D = 160 nm at which I_{sc} is optimized. With increasing D, the $j_{sc,NW}$ drops and at D = 800 nm, we find $j_{sc,NW}$ = 75 mA/cm^2. For the L = 2000 nm and D = 110 nm, we find $j_{sc,NW}$ = 940 mA/cm^2, which is 30 times higher than the limit of j_{sc} = 31 mA/cm^2 in a bulk InP solar cell [17] (note that a high short-circuit current density of >800 mA/cm^2 was found also in a previous modeling study of InP nanowires of 112 nm in diameter [18]). If we assume the V_{oc} = 0.779 V and FF = 0.724 measured for an InP nanowire array solar cell [1], we find the apparent efficiency $\eta = V_{oc}j_{sc,NW}FF/P_{inc}$ = 590 % with P_{inc} = 900 W/m^2 the incident intensity of the AM1.5D spectrum. The absorption in the single nanowire increases with increasing nanowire length, without bound as discussed in connection to Figure 1(a). With D = 110 nm and L > 3500 nm, due to increased absorption, we predict an apparent efficiency in excess of 1000 % (see Supplementary Information Figure S3).

A natural question to ask is how such an >100 % apparent efficiency for a single nanowire affects the performance of the corresponding large-area nanowire-array. We modeled for varying period P the absorption in an array of the above nanowires of D = 110 nm and L = 2000 nm (Figure 6). First, we notice that the $j_{sc,array}$ peaks at 26 mA/cm^2 at the very small period of P = 140 nm and drops monotonously with increasing P (Figure 6(a)). Second, the nanowires in this array show $j_{sc,NW}$ = 53 mA/cm^2 at this P =140 nm, which is 18 times lower than the 940 mA/cm^2 of the single nanowire, and $j_{sc,NW}$ increases with increasing P until a peak of 1000 mA/cm^2 at P = 1300 nm is reached (Figure 6(b)). After this peak, with increasing P, $j_{sc,NW}$ convergences towards the $j_{sc,NW}$ = 940 mA/cm^2 of the single nanowire. Thus, $j_{sc,array}$ and $j_{sc,NW}$ show opposite dependence on P.

To understand this opposite behavior of $j_{sc,array}$ and $j_{sc,NW}$, we show the absorptance A of the array in Figure 6(c) and the corresponding absorption cross-section σ_{abs} of each nanowire in Figure 6(d). For the small $P \approx$ 140 nm, the array shows A close to 1 in a broad wavelength range (Figure 6(c)). With increasing P toward 900 nm, the absorptance at the HE_{11} peak at $\lambda \approx$ 620 nm stays high, but the absorptance drops outside of this peak compared to the values at P = 140 nm. Due to this drop, $j_{sc,array}$ drops. With further increase of P beyond 1000 nm, the absorptance also at this peak wavelength drops. In contrast, the absorption cross-section σ_{abs} of each nanowire at the HE_{11} peak at $\lambda \approx$ 620 nm drops with decreasing P when P < 1000 nm. Hence, the large absorption cross-section observed for the individual nanowires at the HE_{11} peak, which drives the large $j_{sc,NW}$, cannot be fully utilized to boost the absorptance of the array when optimizing $j_{sc,array}$ — the competition in absorption between neighboring nanowires sets in before P is decreased enough to enhance $A(\lambda)$ outside of the HE_{11} peak to optimize $j_{sc,array}$.

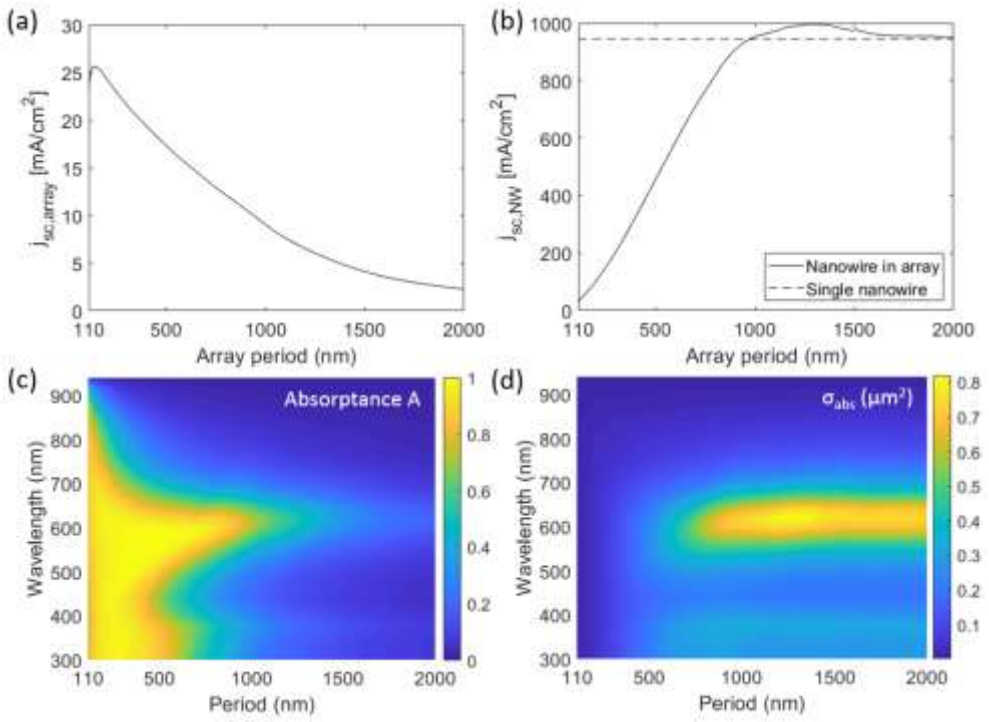

Figure 6. Absorption of light as a function of period for an InP nanowire array of D = 110 nm and L = 2000 nm. (a) Short-circuit current density $j_{sc,array}$ of the array, calculated from Eq. (2) with the absorptance A shown in (c). (b) The short-circuit current density $j_{sc,NW}$ through the cross-section of each nanowire in the array, as calculated from the absorption cross-section in (d), which is in turn calculated as $\sigma_{abs} = P^2A$ from the A in (c). Here, the $j_{sc,NW}$ of the single nanowire in Figure 5(b) is shown with the dashed line.

Thus, $P \approx 1000$ nm appears as the period above which the absorptance of the array at the HE_{11} peak at $\lambda \approx 620$ nm drops and below which the σ_{abs} at $\lambda \approx 620$ nm drops. At this λ = 620 nm, we calculated for the single nanowire of D = 110 nm, similarly as in Section 3.1 for D = 160 and 180 nm, an in-coupling equivalent to 110 times σ_{geom} and an absorption length of 7500 nm for the HE_{11} guided mode. Thus, if we pack the nanowires closer in an array than giving each nanowire a unit cell with area corresponding to 110 times σ_{geom}, we could expect the I_{sc} per nanowire to drop due to competition in the in-coupling into the HE_{11} mode per nanowire. Indeed, for this D = 110 nm, $\sigma_{coupling}/\sigma_{geom} = 110$ corresponds to P = 975 nm, in excellent agreement with the $P \approx 1000$ nm below which neighboring nanowires start to compete noticeably for absorption of light at $\lambda \approx 620$ (Figure 6(d)).

Therefore, in order to not limit the absorption per nanowire, we cannot pack the nanowires closer than 1000 nm apart. For the D = 110 nm, such a packing density corresponds to an area coverage of 1%. The single nanowire showed at L = 2000 nm a 30 times higher $j_{sc,NW}$ than the 31 mA/cm^2 bulk limit. When considering the 1% packing density at P = 1000 nm, we expect $j_{sc,array} \approx 30 \times 31/100 = 9.3$ mA/cm^2, in good agreement with the modeling in Figure 6(a)).

Thus, $j_{sc,array}$ is not optimized with nanowires that optimize $j_{sc,NW}$. Instead, the way to optimize $j_{sc,array}$ is to place the HE_{11} absorption peak close to the bandgap wavelength with $D \approx 180$ nm (for InP nanowires) and then tune the period to enhance the absorption at shorter wavelengths - see Supplementary Information Figure S4 for an example and comparison to the single nanowire absorption for D = 180 nm and L = 2000 nm. There, the optimum period is P = 350 nm, considerably larger than the optimum P = 140 nm for D = 110 nm.

3.4 Comparison to a single GaAs and a single Si nanowire

Finally, we comment on how the choice of the nanowire material affects $j_{sc,NW}$, which showed high values in excess of 900 mA/cm^2 for an InP nanowire of 110 nm in diameter (Figure 5(c)). The optical properties of the nanowire are determined by the refractive index n of the nanowire material. Re(n) affects the diffraction of light and hence the location of the absorption peak of the HE_{1m} modes [25]. For a fixed diameter, the absorption peak red-shifts with increasing Re(n). Im(n) affects in turn mostly the absorption strength of the material and hence the $j_{sc,NW}$ that can be reached for given nanowire diameter and length.

Furthermore, the bandgap of the material affects the wavelength range from which the material can absorb photons to photogenerate carriers. InP shows a bandgap wavelength of approximately 925 nm (1.34 eV), GaAs 873 nm (1.42 eV), and Si 1107 nm (1.12 eV), and all three materials yield a close to maximum efficiency limit for a single junction solar cell [17]. As calculated from Eq. (2) with A = 1 for $\lambda < \lambda_{bg}$, the bulk limit on the short-circuit current is 39 mA/cm^2 for Si, as compared to the 31 mA/cm^2 for InP and 28 mA/cm^2 for GaAs (in contrast, due to their higher bandgap, GaAs and InP show higher limit on open-circuit voltage, resulting in a similar limit on efficiency as for Si).

Furthermore, InP, GaAs, and Si show similar Re(n) in the range of 3-4 for $\lambda > 500$ nm. However, InP and GaAs are direct bandgap semiconductors that show rather large Im(n) almost all the way to the bandgap wavelength. For InP with λ_{bg} = 925 nm, Im(n) > 0.1 for $\lambda < 900$ nm and Im(n) > 0.3 for $\lambda < 650$ nm [19]. For GaAs, we find similarly high values for Im(n), which are approximately 30% lower than for InP [26]. In contrast, Si is an indirect semiconductor that shows low Im(n) in a broad wavelength range. For Si, Im(n) < 0.05 for $\lambda > 500$ nm and Im(n) < 0.01 for $\lambda >700$ nm [27]. Due to this difference in Im(n), for a given nanowire length and diameter, an InP or GaAs nanowire can generate noticeably higher $j_{sc,NW}$ than a Si nanowire (Figure 5c and Supplementary Information Figure 5), even though bulk Si shows the prospect of higher j_{sc} thanks to its lower bandgap. The difference is apparent when considering the absorption cross-section σ_{abs} of the InP, GaAs, and Si nanowire (Figure 5(a) and Supplementary Information Figure 5). The InP and GaAs nanowire show large values of σ_{abs} at the HE_{1m} peaks almost all the way to the bandgap wavelength. Also the Si nanowire shows a peak due each of

the HE_{1m} modes, similarly as found for a sparse array of Si nanowires [28]. However, for $\lambda > 500$ nm, with increasing wavelength, the Si nanowire shows rapidly dropping values in σ_{abs} even at these peaks due to the rapid drop in Im(n).

All three materials show a distinct peak in $j_{sc,NW}$ due to the absorption peak from the HE_{11} mode (Figure 5(c) and Supplementary Information Figure 5). For GaAs, we find a peak of $j_{sc,NW} = 840$ at $D = 100$ nm, which is rather comparable to the results for InP — for both materials, at the peak diameter, the peak in σ_{abs} shows up at $\lambda \approx$ 600-650 nm. However, for Si, the peak in $j_{sc,NW}$ shows up at a considerably smaller diameter of $D = 60$ nm where $j_{sc,NW} = 290$ mA/cm^2, considerably lower than for InP and GaAs. Furthermore, at this $D = 60$ nm, the HE_{11} absorption peak for the Si nanowire shows up at a noticeably shorter wavelength of $\lambda \approx 450$ nm than for the InP and GaAs nanowire, indicating that the $j_{sc,NW}$ of the Si nanowire is optimized when the HE_{11} absorption peak is pushed into the short-wavelength region of higher Im(n).

4. Conclusions

We compared the absorption in a single vertical nanowire and the corresponding nanowire array. The single nanowire can show a remarkably high short-circuit current density, thanks to which we predict an apparent solar cell efficiency in excess of 500%. This high short-circuit current density originates from a very high absorption cross-section at an absorption peak. At such a peak, the absorption cross-section can be more than 50 times larger than the geometrical cross-section. Thus, the nanowire absorbs light from a large surrounding and, after optimizing the diameter, shows more than 30 times higher short-circuit current density than a bulk solar cell. Hence, the single vertical nanowire is a very interesting component for miniaturized photovoltaics.

However, it is not trivial to utilize such a very high short-circuit current density of a single nanowire in a large-area nanowire-array solar cell. In a large-area solar cell, we aim to absorb all the above-bandgap photons. To enhance the absorption at wavelengths outside of the absorption peak of the single nanowire, the nanowires must be packed rather close to each other. Then, at the absorption peak, neighboring nanowires compete strongly for absorption of incident photons, and the absorption per nanowire at the peak decreases dramatically. As an end result, the optimum diameter for the nanowire array is considerably different from that for the single, individual nanowire (in our case of InP nanowires, the optimum diameter is 180 nm for the array and 110 nm for the single nanowire). Thus, the design guidelines for optimizing the short-circuit current density cannot be directly transferred between a single nanowire and a nanowire array.

Acknowledgements

This work was supported by the Academy of Finland (grant number 286920).

References

[1] Wallentin J, Anttu N, Asoli D, Huffman M, Aberg I, Magnusson MH, Siefer G, Fuss-Kailuweit P, Dimroth F, Witzigmann B, Xu HQ, Samuelson L, Deppert K, Borgstrom MT. 2013 InP nanowire array solar cells achieving 13.8% efficiency by exceeding the ray optics limit. Science ***339*** 1057-1060.

[2] Åberg I, Vescovi G, Asoli D, Naseem U, Gilboy JP, Sundvall C, Dahlgren A, Svensson KE, Anttu N, Björk MT. 2016 A GaAs nanowire array solar cell with 15.3% efficiency at 1 sun. IEEE J. Photovolt. ***6*** 185-190.

[3] Otnes G, Borgström MT. 2017 Towards high efficiency nanowire solar cells. Nano Today ***12*** 31-45.

[4] van Dam D, van Hoof NJ, Cui Y, van Veldhoven PJ, Bakkers EP, Gómez Rivas J, Haverkort JE. 2016 High-efficiency nanowire solar cells with omnidirectionally enhanced absorption due to self-aligned indium–tin–oxide mie scatterers. ACS Nano ***10*** 11414-11419.

[5] Krogstrup P, Jørgensen HI, Heiss M, Demichel O, Holm JV, Aagesen M, Nygard J, i Morral AF. 2013 Single-nanowire solar cells beyond the Shockley–Queisser limit. Nat. Phot. ***7*** 306.

[6] LaPierre R, Robson M, Azizur-Rahman K, Kuyanov P. 2017 A review of III–V nanowire infrared photodetectors and sensors. J. Phys. D ***50*** 123001.

[7] Anttu N, Xu H. 2013 Efficient light management in vertical nanowire arrays for photovoltaics. Opt. Express ***21*** A558-A575.

[8] Anttu N. 2013 Geometrical optics, electrostatics, and nanophotonic resonances in absorbing nanowire arrays. Opt. Lett. ***38*** 730-732.

[9] Huang N, Lin C, Povinelli ML. 2012 Broadband absorption of semiconductor nanowire arrays for photovoltaic applications. J. Opt. ***14*** 024004.

[10] Kupec J, Witzigmann B. 2009 Dispersion, wave propagation and efficiency analysis of nanowire solar cells. Opt. Express ***17*** 10399-10410.

[11] Diedenhofen SL, Janssen OT, Grzela G, Bakkers EP, Gómez Rivas J. 2011 Strong geometrical dependence of the absorption of light in arrays of semiconductor nanowires. ACS Nano ***5*** 2316-2323.

[12] Anttu N, Abrand A, Asoli D, Heurlin M, Åberg I, Samuelson L, Borgström M. 2014 Absorption of light in InP nanowire arrays. Nano Res. ***7*** 816-823.

[13] Yang Y, Peng X, Hyatt S, Yu D. 2015 Broadband quantum efficiency enhancement in high index nanowire resonators. Nano Lett. ***15*** 3541-3546.

[14] Seo K, Wober M, Steinvurzel P, Schonbrun E, Dan Y, Ellenbogen T, Crozier KB. 2011 Multicolored vertical silicon nanowires. Nano letters ***11*** 1851-1856.

[15] Bures J. Guided Optics: Optical Fibers and All-Fiber Components. (Wiley-VCH, 2008).

[16] Green MA, Hishikawa Y, Dunlop ED, Levi DH, Hohl-Ebinger J, Ho-Baillie AW. 2018 Solar cell efficiency tables (version 52). Prog. Photovolt. Res. Appl. ***26*** 427-436.

[17] Shockley W, Queisser HJ. 1961 Detailed balance limit of efficiency of p-n junction solar cells. J. Appl. Phys. ***32*** 510-519.

[18] Wenas YC, Mokkapati S, Tan HH, Jagadish C. 2014 Extremely high short-circuit current density in vertical single nanowire solar cells. 2014 Conference on Optoelectronic and Microelectronic Materials & Devices, Perth, WA, 2014, 77-78.

[19] Glembocki OJ, Piller H. *Indium Phosphide (InP)* in Handbook of Optical Constants of Solids, E. D. Palik, ed. (Academic, 1985): 503-516.

[20] Anttu N, Xu H. 2011 Scattering matrix method for optical excitation of surface plasmons in metal films with periodic arrays of subwavelength holes. Phys. Rev. B ***83*** 165431.

[21] Hessel A, Oliner A. 1965 A new theory of Wood's anomalies on optical gratings. Appl. Opt. ***4*** 1275-1297.

[22] Mokkapati S, Saxena D, Tan HH, Jagadish C. 2015 Optical design of nanowire absorbers for wavelength selective photodetectors. Sci. Rep. ***5*** 15339.

[23] Reference Solar Spectral Irradiance: ASTM G-173. Available at: https://rredc.nrel.gov/solar/spectra/am1.5/ASTMG173/ASTMG173.html, 2018.

[24] Otnes G, Barrigón E, Sundvall C, Svensson KE, Heurlin M, Siefer G, Samuelson L, Åberg I, Borgström MT. 2018 Understanding InP nanowire array solar cell performance by nanoprobe-enabled single nanowire measurements. Nano Lett. ***18*** 3038-3046.

[25] Anttu N, Lehmann S, Storm K, Dick KA, Samuelson L, Wu PM, Pistol M. 2014 Crystal phase-dependent nanophotonic resonances in InAs nanowire arrays. Nano Lett. ***14*** 5650-5655.

[26] Palik ED. *Gallium Arsenide (GaAs)* in Handbook of Optical Constants of Solids, E. D. Palik, ed. (Academic, 1985): 429-443.

[27] Green MA. 2008 Self-consistent optical parameters of intrinsic silicon at 300 K including temperature coefficients. Sol. Energy Mater Sol. Cells ***92*** 1305-1310.

[28] Wang B, Leu PW. 2012 Tunable and selective resonant absorption in vertical nanowires. Opt. Lett. ***37*** 3756-3758.